Surface-Directed Spinodal Decomposition on a Macroscopic Scale in a Nitrogen and Carbon Alloyed Steel

Barbara Aichmayer,[1,*] Peter Fratzl,[1] Sanjay Puri,[2] and Gabriele Saller[3]

[1]*Erich Schmid Institute of Materials Science, Austrian Academy of Sciences & University of Leoben, A-8700 Leoben, Austria*

[2]*School of Physical Sciences, Jawaharlal Nehru University, New Delhi 110067, India*

[3]*Böhler Edelstahl GmbH & Co KG, A-8605 Kapfenberg, Austria*

(Received 11 July 2002; published 2 July 2003)

Interactions with the macroscopic specimen surface can profoundly modify phase-separation processes. This has previously been observed in liquids and polymer films and is theoretically described by the theory of surface-directed spinodal decomposition (SDSD). Here we report first observations of SDSD in a metallic alloy on a macroscopic scale. The influence of the surface leads to the development of concentric domains extending over the whole 10 mm thick cylindrical steel specimen, due to long-range interactions via elastic stresses and long-range diffusion of the interstitial elements nitrogen and carbon.

DOI: 10.1103/PhysRevLett.91.015701 PACS numbers: 64.75.+g, 68.35.Dv, 81.30.Mh

By a rapid change of system parameters (e.g., temperature, pressure) a multicomponent mixture can be brought from the one-phase region into a homogeneous initial state which is thermodynamically unstable. The system then undergoes phase separation and the late stages of this process are characterized by the coarsening of single-phase domains [1]. In the presence of a surface, the phase-separation process may be modified due to the wetting tendency of the surface by one of the phases [1–5]. This results in the formation of anisotropic surface-directed concentration waves which form a layered structure parallel to the surface. This effect has attracted much experimental and theoretical interest and has been referred to as *surface-directed spinodal decomposition* (SDSD) [1–5]. However, we should stress that the usage of the term "spinodal decomposition" in this context also includes the possibility of phase separation via nucleation and growth [1,6]. The primary interest here is the asymptotic nature of domain growth, where the distinction between the two routes to phase separation is not physically relevant. Earlier experiments on this problem have focused on polymer and fluid mixtures [2,3]. In this Letter, we present the first experimental observation of SDSD in solid mixtures, i.e., commercial steels.

The precipitation of ferrite (δ, bcc) in an austenitic (γ, fcc) stainless steel at 1325 °C was studied. Table I shows the composition of the investigated alloy. The steel contained the interstitial alloying elements nitrogen (N) and carbon (C), which strongly stabilize the austenitic structure. The substitutional alloying elements, chromium (Cr) and molybdenum (Mo), are ferrite-stabilizing elements. However, the effect of the alloying element manganese (Mn) depends on the composition. Usually, Mn is considered to stabilize austenite, but especially in nitrogen-alloyed steels, at high concentrations of more than approximately 10%, Mn acts as a ferrite former [7]. The Mn content of the investigated steel is equivalent to this limit.

In order to obtain a single-phase austenitic structure, the steel was solution annealed at 1100 °C (see Fig. 1) for 1 h and quenched in water. Then cylindrical samples of diameter 10 mm were sealed under vacuum in silica ampoules to ensure a well-defined, nonoxidizing atmosphere during the subsequent heat treatment at 1325 °C. After rapid heating and annealing for 6, 12, 24, and 48 h in the two-phase region $\delta + \gamma$, the samples were again quenched in water. The resulting structures (Fig. 2) show a sample-shape dependent macroscopic decomposition perpendicular to the surface. The homogeneous initial structure (0 h, only solution treated) consists of fine grains of austenite. In the second sample (6 h), a rather fine-grained two-phase $\delta + \gamma$ domain in the center is surrounded by successive layers of coarse grains of austenite (γ) and ferrite (δ). After 12 h of annealing, the outermost layer consisting of ferrite has propagated into the bulk and the central $\delta + \gamma$ region has vanished. The corresponding picture for 48 h illustrates the further growth of the δ-wetting layer (see also Fig. 4).

From wavelength-dispersive x-ray measurements, the N and C contents of the austenitic domain were found to be 1.6 times higher than the corresponding values for the ferritic layer. Using energy-dispersive x-ray analysis, it was observed that the austenitic phase contained 1.5 times more Mn than the ferritic region. Regarding the investigated steel, Mn obviously stabilizes the austenitic structure in the center of the samples. In contrast with Mn, other substitutional elements such as Cr and Mo did not show any concentration variations. The measured composition of the different phases differs strongly from the calculated bulk equilibrium ratios for γ:δ [8] (4:1 for N

TABLE I. Chemical composition of the tested steel.

N (wt %)	C (wt %)	Cr (wt %)	Mn (wt %)	Mo (wt %)	Fe
0.30	0.15	16	10	2	Balance

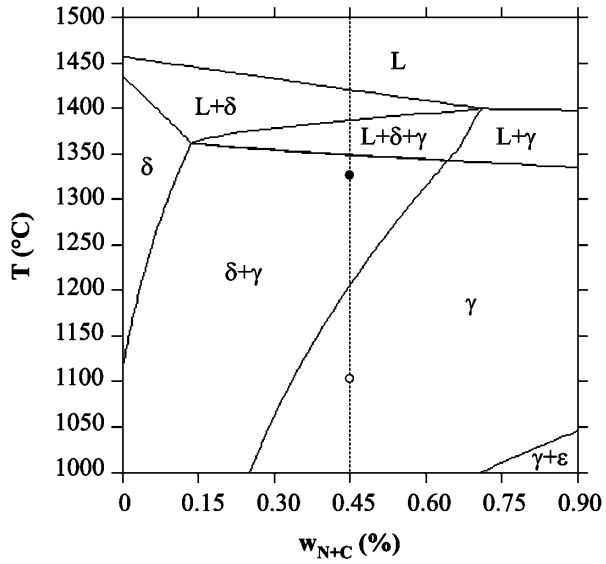

FIG. 1. Temperature against weight of nitrogen + carbon. Phase diagram of the multicomponent system for w_N:w_C = 2:1, calculated using the program THERMO-CALC [8]. Phase domains are shown for L, liquid; δ, ferrite; γ, austenite; ϵ, Cr_2N. The vertical line indicates the composition of the tested steel. The specified temperatures are as follows: ○, solution treatment at 1100 °C; ●, annealing at 1325 °C.

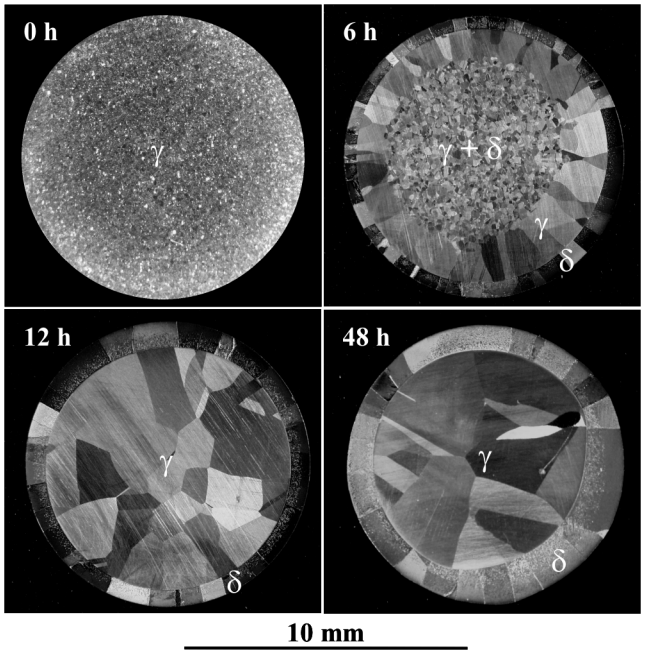

FIG. 2. Sample-shape dependent structure of cylindrical steel samples for different annealing times: 0 h (only solution treated), 6, 12, and 48 h. The annealing temperature was 1325 °C. The ferrite phase is δ, and the austenite phase is γ.

and C, 1.1:1 for Mn, 1:1.1 for Cr, 1:1.3 for Mo). We repeated the experiment with a steel having a composition slightly different from the one given in Table I (1.1% copper added), and this gave results very similar to those described above.

The results in Fig. 2 constitute a realization of SDSD in the context of solid mixtures, where diffusion drives segregation. Essentially, there are two reasons why the ferrite phase (δ) is preferentially attracted to the open surface, viz., the atmosphere in the silica ampoules, and the stress caused by the phase transformation $\gamma \rightarrow \delta$. First, during the heat treatment at 1325 °C, some of the interstitial N atoms leave the solid steel sample and form nitrogen gas (N_2). Because of the hermetically sealed atmosphere in the silica ampoule, the rising N_2 pressure will soon prevent further evaporation. An estimation using the saturation pressure of nitrogen in the ampoule indicates a negligible nitrogen loss in the specimen. Nevertheless, the ambient N_2 pressure pins the N content in the surface regions to its equilibrium value in the δ phase. The second important factor is the rather large volume expansion (9%), which accompanies the transformation of austenite (fcc) into ferrite (bcc). The dilation of the ferritic wetting layer results in stresses, building up a long-ranged elastic field which makes it energetically advantageous for the ferrite structure to be at the outer boundary.

The following numerical simulation in $d = 2$ clarifies the analogy between the structural evolution in Fig. 2 and the late stages of SDSD with a long-ranged surface field. The simulation is based on the standard Cahn-Hilliard-Cook equation for a binary (AB) mixture [4,9–11] in polar coordinates (R, ϕ):

$$\frac{\partial \psi}{\partial \tau} = -\nabla^2\left[\psi - \psi^3 + \frac{1}{2}\nabla^2\psi + V(R)\right] + \vec{\nabla}\cdot\vec{\xi} \equiv -\vec{\nabla}\cdot\vec{J}. \quad (1)$$

The rescaled order parameter $\psi(R, \phi, \tau)$ differentiates between the A-rich and the B-rich phases, where $\psi = +1$ and -1, respectively. It is a function of dimensionless space (R, ϕ) and time τ. The space variable is rescaled by the bulk correlation length $\ell_b = (1 - T/T_c)^{-1/2}$, where T is the quench temperature and T_c is the critical temperature [4]. In Eq. (1), $\vec{\xi} = (\xi_R, \xi_\phi)$ is a Gaussian random current, and $\vec{J}$ denotes the current or flux which drives the order-parameter evolution. The surface potential $V(R)$ on the preferred component of the mixture is described by a power law: $V(R) = h_1(R_0 - R)^{-n}$ for $R_0 - R > 1$, and $V(R) = h_1$ for $R_0 - R \leq 1$, where R_0 is the system radius. The exponent n depends on the interaction range, with $n = 1$ being appropriate in the context of long-ranged strain fields [1]. Equation (1) is supplemented by two boundary conditions at the surface ($R = R_0$):

$$\frac{\partial \psi(R_0, \phi, \tau)}{\partial \tau} = h_1 + g\psi(R_0, \phi, \tau) + \gamma \frac{\partial \psi(R, \phi, \tau)}{\partial R}\bigg|_{R=R_0}, \quad (2)$$

$$0 = \left\{ \frac{\partial}{\partial R} \left[\psi(R, \phi, \tau) - \psi(R, \phi, \tau)^3 + \frac{1}{2}\nabla^2 \psi(R, \phi, \tau) + V(R) \right] - \xi_R(R, \phi, \tau) \right\} \Big|_{R=R_0}. \quad (3)$$

The boundary condition in Eq. (2) rapidly drives the order parameter at the surface to its equilibrium value, and Eq. (3) is the no-flux condition for the radial current. The parameters g and γ are related to the bulk correlation length [4]. A lower limit on R (say, R_m) is necessary to avoid the singularity at $R = 0$ in the Laplacian, which is $\nabla^2\psi = (\partial^2\psi/\partial R^2) + (1/R)(\partial\psi/\partial R) + (1/R^2)(\partial^2\psi/\partial\phi^2)$ in polar coordinates (R, ϕ). This small R cutoff is treated in the following way in the simulations: the neighbor of a point at (R_m, ϕ) is the point at $(R_m, \phi + \pi)$. Figure 3 shows evolution pictures obtained from a simulation of Eqs. (1)–(3), and these are analogous to the experimental snapshots shown in Fig. 2. The parameter values in our simulation were $g = -4$ and $\gamma = 4$. The surface field was characterized by the field strength $h_1 = 8$ and the exponent $n = 1$. The discretization mesh sizes in space and time were $(\Delta R = 1, \Delta\phi = \pi/25)$ and $\Delta\tau = 0.005$, respectively. The lattice size was fixed as $R_0 = 100$, and we set $R_m = 4$. The initial condition for the evolution consisted of random small-amplitude fluctuations about an average value of $\psi_0 = -0.2$. The phase with $\psi > 0$ wets the surface, so the wetting component is the minority phase in our simulations. This is in accordance with our experimental system, whose phase diagram is shown in Fig. 1. The morphological evolution in Fig. 2 (or Fig. 3) can be quantified by examining the growth dynamics of the wetting layer. Figure 4 shows the time dependence of the wetting-layer thickness, L_W, in our experiments (denoted as filled circles) and simulations (denoted as a solid line). To facilitate comparison, the wetting-layer thickness was normalized by the system radius, 5 mm (steel sample) and 100 (simulation lattice, nondimensional), respectively. The (nondimensional) time $\tau = t/t_0$ from the simulation data was multiplied by a diffusion time $t_0 = 26.4$ s in order to fit the real time t from the experimental data. The growth of the ferritic wetting layer exhibits the same features as the numerical result, starting with rapid initial growth and finally reaching a plateau. There are additional physical effects, not accounted for in our simulation, which can affect phase-separation kinetics in our experimental system and cause quantitative deviations between the calculated and measured data. Nevertheless, comparing the experimental (Fig. 2) and numerical (Fig. 3) results, the qualitative similarity of the structural evolution becomes obvious. In both cases, the propagating wetting layer finally dominates over domain growth in the bulk.

Further influences on the decomposition behavior in our experiments need to be discussed with regard to the role of the alloying elements. For instance, both external and internal stresses affect phase separation. Stress not only influences the thermodynamic equilibrium via the contribution of elastic energy to the overall free energy, but also changes the diffusion kinetics. Furthermore, the long-range nature of elastic forces results in nonlocal effects in the diffusion equation [12]. The effect of stress on spinodal decomposition has been the topic of various

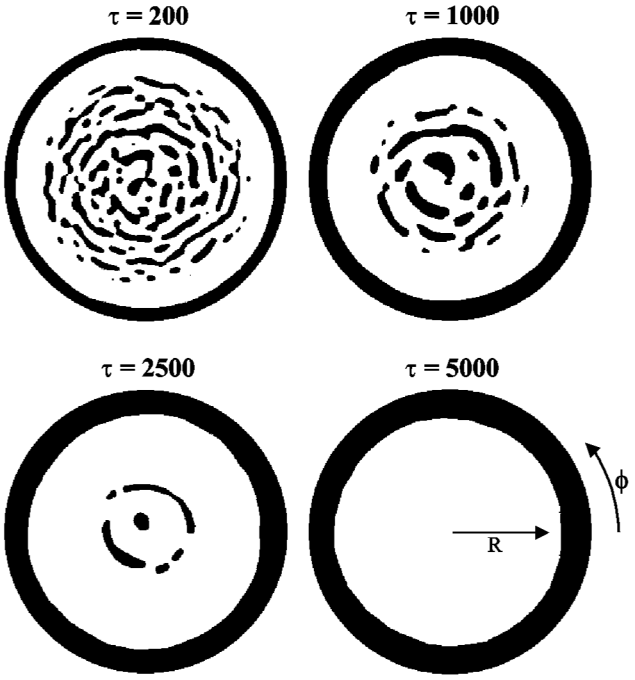

FIG. 3. Evolution pictures obtained from a simulation of Eqs. (1)–(3), at four dimensionless times. Details of the simulation are provided in the text. Lattice sites with $\psi < 0$ are unmarked, and lattice sites with $\psi \geq 0$ are marked in black.

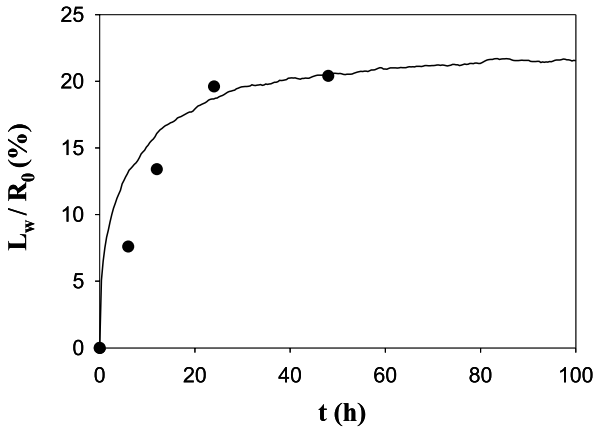

FIG. 4. Ratio of the thickness of the wetting layer to the system radius, L_W/R_0 (%), as a function of time t (h). The filled circles show experimental values for the investigated steel samples, and the solid line was obtained from the simulation depicted in Fig. 3. The numerically observed (nondimensional) time $\tau = t/t_0$ was multiplied by $t_0 = 26.4$ s to fit the experimental data.

studies (for recent reviews, see [1,13]). Recently, Johnson [14] discussed the interplay of external stress and compositional strain. He modeled spinodal decomposition in a small radially stressed sphere, and obtained a microstructure consisting of a series of concentric layers. Experiments on hydrogen-metal systems by Tretkowski *et al.* [15] studied a very interesting related phenomenon. A spatially varying interstitial concentration caused a varying lattice expansion which led to coherency stresses. These stresses provoked macroscopic decomposition modes which depended on the boundary conditions, e.g., the shape of the crystal. Zabel and Peisl [16] investigated the sample-shape-dependent coherent α-α' phase transition of hydrogen (H) in niobium (Nb) for different geometries. They used wires of diameter 1.2 mm, which showed a structure very similar to the one observed in our experiments with cylindrical steel samples of diameter 10 mm. The α' phase was located in the core, and surrounded by the α phase at the cylinder wall. Furthermore, it was suggested that for all geometries, wetting behavior may be superimposed on the coherent spinodal decomposition. In the context of our experiment on steel, the interstitials N and C take the place of H in Nb. Both elements strongly dilate the lattice, with nitrogen causing a higher lattice dilation than carbon [17]. In comparison with the interstitials, the dilation due to the substitutional elements Cr, Mn, and Mo is rather small. As we have mentioned before, the transformation of ferrite into austenite is incoherent. Nevertheless, stresses play a crucial role in our investigation because both coherent and incoherent decomposition interfere with each other, resulting in the observed structure.

It is also relevant to examine the effects of thermal transport in our experiments. A simple estimate using the independently measured thermal diffusivity of the material (5.4×10^{-6} m^2/s at 1325 °C) shows that temperature gradients over the radius of the specimen disappear in seconds. Thus, the thermalization time is orders of magnitude smaller than our annealing times (6–48 h), and thermal transport is not likely to play an important role in the phase-separation process.

Finally, the macroscopic nature of the decomposition phenomenon, which can easily be seen with the naked eye (Fig. 2), is intimately related to the role of interstitial atoms. Indeed, the very large scale of phase separation requires diffusion lengths of the same order of magnitude as the sample dimension of 10 mm. This condition can be met by the interstitial elements (N, C). In spite of the high annealing temperature (1325 °C) and the long annealing times (up to 2 d), it is less obvious why the substitutional element Mn shows some concentration variations and, therefore, also a diffusion length in the mm range. Mn and interstitials (N, C) attract each other, N having a stronger interaction with Mn than C [18]. Since other elements such as Cr and Mo remain uniformly distributed, it may be postulated that there exists a fast diffusion path for Mn, possibly involving vacancies and/or interstitial complexes with Mn atoms.

In conclusion, we have presented the first experimental study of surface-directed spinodal decomposition in solid mixtures, viz., stainless steel alloyed with N and C. We find that our experiments are in a qualitative agreement with a model for SDSD adapted to cylindrical geometry. Our investigations highlight the importance of the specimen shape and surface for the phase-separation process, even in macroscopic solid alloys, when both the range of interaction and the diffusion lengths are sufficiently large. In the present example, this is realized by elastic strain interactions and interstitial diffusion.

*Electronic address: aichmayer@unileoben.ac.at

[1] K. Binder and P. Fratzl, *Spinodal Decomposition*, in Phase Transformations in Materials, edited by G. Kostorz (Wiley-VCH, Weinheim, 2001), p. 409.
[2] R. A. L. Jones, L. J. Norton, E. J. Kramer, F. S. Bates, and P. Wiltzius, Phys. Rev. Lett. **66**, 1326 (1991).
[3] G. Krausch, Mater. Sci. Eng., R **14**, 1 (1995).
[4] S. Puri and H. L. Frisch, J. Phys. Condens. Matter **9**, 2109 (1997).
[5] K. Binder, J. Non-Equilib. Thermodyn. **23**, 1 (1998).
[6] J.W. Cahn, Trans. Metall. Soc. AIME **242**, 166 (1968).
[7] P. J. Uggowitzer, R. Magdowski, and M. O. Speidel, ISIJ International **36**, 901 (1996).
[8] All computations of the equilibrium state were performed using the program THERMO-CALC and the database TCFE2000 from Thermo-Calc Software, Stockholm, Sweden; J. O. Andersson, T. Helander, L. Hoglund, S. Pingfang, and B. Sundman, Calphad **26**, 273 (2002).
[9] S. Puri and K. Binder, Phys. Rev. A **46**, R4487 (1992).
[10] S. Puri, K. Binder, and H. L. Frisch, Phys. Rev. E **56**, 6991 (1997).
[11] S. Puri and K. Binder, Phys. Rev. Lett. **86**, 1797 (2001).
[12] F. C. Larché and J.W. Cahn, Acta Metall. **33**, 331 (1985).
[13] P. Fratzl, O. Penrose, and J. L. Lebowitz, J. Stat. Phys. **95**, 1429 (1999).
[14] W. C. Johnson, Acta Mater. **49**, 3463 (2001).
[15] J. Tretkowski, J. Völkl, and G. Alefeld, Z. Phys. B **28**, 259 (1977).
[16] H. Zabel and H. Peisl, Phys. Rev. Lett. **42**, 511 (1979).
[17] V. G. Gavriljuk and H. Berns, *High Nitrogen Steels* (Springer, Berlin, 1999).
[18] A. L. Sozinov and V. G. Gavriljuk, Scr. Mater. **41**, 679 (1999).